Biochemistry

 Volume 38, Number 7 February 16, 1999

Accelerated Publications

Millisecond to Microsecond Time Scale Dynamics of the Retinoid X and Retinoic Acid Receptor DNA-Binding Domains and Dimeric Complex Formation†

Paul J. A. van Tilborg,‡ Frans A. A. Mulder,‡ Maaike M. E. de Backer,‡ Margie Nair,‡,§ Erika C. van Heerde,|| Gert Folkers,‡ Paul T. van der Saag,|| Yasmin Karimi-Nejad,‡ Rolf Boelens,‡ and Robert Kaptein*,‡

Bijvoet Center for Biomolecular Research, NMR Spectroscopy Department, Utrecht University, Padualaan 8, NL-3584 CH, Utrecht, The Netherlands, and Hubrecht Laboratory, Netherlands Institute for Developmental Biology, Uppsalalaan 8, NL-3584 CT, Utrecht, The Netherlands

Received October 22, 1998; Revised Manuscript Received December 11, 1998

ABSTRACT: The all-trans retinoic acid and 9-cis retinoic acid receptors (RAR and RXR, respectively) belong to a family of ligand inducible transcription factors, which exert their effect via binding to hormone response elements. Both are members of the class II sub-family of nuclear receptors, which bind DNA as dimers, on tandem repeats of a hexamer motif separated by a variable spacer. The variability in spacer length and the head-to-tail organization of the hormone response elements result in different protein−protein interactions in each of the complexes. We show that the zinc-coordinating loop regions of RXR and RAR DNA-binding domains exhibit dynamics on the millisecond to microsecond time scale. The highly dynamic second zinc finger of RXR constitutes the primary protein−protein interface in many nuclear receptor assemblies on DNA. Dynamics is also observed in the first and second zinc fingers of RAR, which are implicated in dimeric interactions with RXR on response elements with spacers of 5 base pairs and 1 base pair, respectively. The striking correspondence between the regions that exhibit conformational exchange and the dimer interfaces of the proteins complexed with DNA suggests a functional role for the dynamics. The observed flexibility may allow the proteins to adapt to various partners and with different orientations upon assembly on DNA. Furthermore, the more extensive dynamics observed for RXR may reflect the greater ability of this protein to modulate its interaction surface since it participates in a wide variety of receptor complexes.

The nuclear receptor proteins are transcription factors that function via ligand-mediated sequence-specific DNA binding. They are organized in three functional domains: the N-terminal domain with trans-activational properties; the C-terminal domain, which exhibits ligand binding as well as dimerization and trans-activational capacity; and the central DNA-binding domain (DBD)[1] which also contains a dimer-

† This research has been financially supported by the council for chemical sciences of The Netherlands organization for scientific research (CW/NWO).

‡ Utrecht University.

§ Current address: Biomolecular Research Institute, NMR Laboratory, 343 Royal Parade, Parkville 3052, Melbourne, Australia.

|| Netherlands Institute for Developmental Biology.

[1] Abbreviations: DBD, DNA-binding domain; CTE, C-terminal extension; RXR, 9-cis retinoic acid receptor; GR, glucocorticoid receptor; ER, estrogen receptor; RAR, all-trans retinoic acid receptor; TR, thyroid hormone receptor; VDR, vitamin D3 receptor; PPAR, peroxisome proliferator activated receptor; DR, direct repeat; HRE, hormone response element; bp, base pair; HSQC, heteronuclear single quantum coherence; CPMG, Carr Purcell Meiboom Gill, R_{ex}, conformational exchange contribution to the transverse relaxation rate; FID, free induction decay; INEPT, insensitive nuclei enhancement by polarization transfer; N-coR, nuclear co-repressor.

10.1021/bi982526q CCC: $18.00
Published on Web 01/27/1999

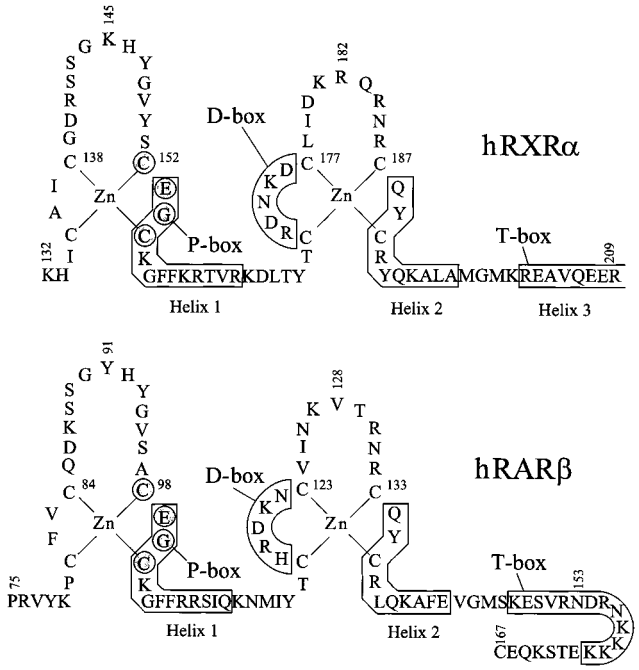

FIGURE 1: Sequence of the RXR and RAR DNA-binding domains. Boxes indicate the helices, D-box and T-box. Grey circles indicate the P-box.

ization function. The DBDs are highly conserved and consist of two repeats of a zinc finger subdomain, forming a 66 residue core, followed by a C-terminal extension (CTE) of about 20 residues. Each zinc finger subdomain consists of a peptide chain, containing four cysteines, which coordinate the zinc ion, immediately followed by a helix (see Figure 1).

On the basis of the DNA-binding properties, the family can be divided into four classes: (i) the steroid hormone receptors, which bind as homo-dimers to DNA sequences made up of palindromic repeats of a hexamer motif; (ii) nonsteroid hormone receptors that bind as heterodimers with the 9-cis retinoic acid receptor (RXR) on direct repeats; (iii) orphan receptors which bind as homo-dimers to direct repeats; and (iv) orphan receptors that bind as monomers to a single half-site (*1*−*4*).

The 3D structures of the glucocorticoid receptor (GR) and estrogen receptor (ER) have provided a detailed picture of the proteins free in solution (*5*−*8*) as well as a wealth of information on protein−DNA and protein−protein interactions (*9*−*11*). A comparison of the structures free in solution with the dimeric structures bound to DNA reveals interesting differences, which are predominantly located in the second zinc finger. Luisi et al. (*8*) were the first to observe that the formation of protein−DNA and protein−protein interactions upon ternary complex formation is accompanied by an ordering of the structure.

In the early nineties, the DNA-binding repertoire of the class II nuclear receptors (e.g., the all-trans retinoic acid receptor (RAR), the thyroid hormone receptor (TR), the vitamin D3 receptor (VDR), and the peroxisome proliferator activated receptor (PPAR)) was elucidated. Their mode of DNA binding differs from that of the steroid hormone receptors in several ways. First, class II nuclear receptors bind to DNA as heterodimers, with RXR as the common upstream partner. Second, the consensus half-sites are ordered as direct repeats (DRs), rather than palindromic sequences. Third, the number of bases between the half-sites, the spacer, is variable in length. The idea that the spacer length is a major determinant in specific DNA recognition gradually evolved to the so-called "1-to-5 rule" (*2*, *12*). According to this rule, DNA-binding specificity of the class II nuclear receptors is as follows: RXR−RXR (DR1), RXR−RAR (DR2, DR5), RXR−VDR (DR3), and RXR-TR (DR4). In addition, other heterodimers are seen on the same direct repeats (e.g., RAR−RXR (DR1) (*13*), RXR−PPAR (DR1) (*14*)). The topology of the hormone response elements (HRE) in this group (a head-to-tail arrangement of half-sites, separated by a variable number of base pairs (bp)) implies that the dimer interface is completely different from the steroid hormone receptors. Mapping of these interfaces indeed showed this to be the case. For the complexes RXR−RXR (DR1) and RXR−RAR (DR2) the second zinc finger, but not the D-box of the upstream RXR, is involved as is the CTE of the downstream component (*15*). In contrast, in complexes of RXR-TR (DR4) and RXR−RAR (DR5) the D-box of the upstream RXR interacts with the prefinger region of TR or the tip of the first finger of RAR (*16*, *17*).

Structural insight at atomic resolution was provided by the solution structures of RXR (*18*, *19*) and RAR (*20*), and by the crystal structure of RXR, cocrystallized with TR and an 18 bp thyroid hormone response element with a 4 bp spacer (DR4) (*21*). Major differences are observed in the zinc finger regions. In the solution structure of RAR, both zinc fingers display considerable disorder compared to the core of the protein. A similar situation is encountered for the solution structure of RXR, where it is the second zinc finger which is ill defined. In contrast to the structure in solution, however, the second zinc finger of RXR, cocrystallized with TR and DR4, is well-ordered. The difference in definition of the dimerization domain between RXR free in solution and in the crystal is reminiscent of the situation encountered for steroid receptors (*5*−*11*). Previous NMR relaxation studies have identified only minor excursions of the protein backbone due to fast (picosecond to nanosecond) dynamics for GR (*22*) and RXR (*19*) free in solution. However, the disorder may manifest itself on other time scales. We present ^{1}H and ^{15}N transverse relaxation data obtained for RXR and RAR DBDs, which show this to be the case. Increased rates were observed for both zinc fingers of RAR and for the second zinc finger of RXR, revealing the presence of substantial and pervasive flexibility on the millisecond to microsecond time scale. The present results provide the first direct observation that the disorder, present in the dimerization domains of RAR and RXR, is due to relatively slow molecular motions. This information may provide additional insight into the disorder-to-order transition, which occurs in the nuclear receptor DBDs upon assembly on DNA.

MATERIALS AND METHODS

Protein Expression and Purification. The expression vector pGEX-2T RXR, with a C195A substitution, was made by standard PCR methods. Expression and purification were performed as described by Lee et al. (*18*), with some modifications. The GST was cleaved from RXR DBD prior to elution from the glutathione-sepharose beads. The eluted RXR DBD was loaded on an Accell Plus column and washed

with buffer A [50 mM Tris (pH 8.0), 1 mM EDTA, 3 mM DTT, 50 mM NaCl, and 5% glycerol]. Subsequently, the RXR DBD was eluted with a linear salt gradient extending from 50 to 800 mM NaCl.

A C-terminally extended hRARβ (75−167) with a C141A substitution was used, which was created by insertion of a PCR fragment in a previously described RAR-DBD expression construct (*20*). The RAR DBD was expressed and purified essentially as described by Knegtel et al. (*20*). However, an extra gel filtration step with a Superdex 75 column and eluting with $TGEDZ_{50}$ with 400 mM NaCl buffer solution was performed.

NMR Spectroscopy and Data Analysis. Samples of RXR and RAR were 2 and 0.5 mM in protein concentration, respectively, dissolved in 95%/5% H_2O/D_2O, pH 6.8, containing 200 mM NaCl, 3 mM DTT, and about 0.1 mM NaN_3. NMR measurements for assignment purposes and relaxation experiments were performed on Varian Unity plus 750 MHz and Bruker AMX/2 600 MHz spectrometers, respectively, operating at 298 K probe temperature. Spectra were processed using NMRPipe (*23*) and analyzed using in-house written software.

Assignments of the $^1H^N$ and ^{15}N resonances, as far as unavailable from Lee et al. (*18*) and Knegtel et al. (*20*), were accomplished according to standard methods (*24*).

^{15}N T_2 relaxation experiments were recorded and analyzed essentially as described before (*25*). ^{15}N and ^1H rf field strengths were 8 and 25 kHz, respectively. 2D data sets were acquired as 80 × 512 (RXR) or 90 × 512 (RAR) complex points with spectral widths of 2200 and 10000 Hz in t_1 (^{15}N) and t_2 (^1H), respectively. Total acquisition times of the series were 30 and 42 h, acquiring 48 and 60 scans per FID, for RXR and RAR, respectively.

Gradient sensitivity-enhanced HSQC and CPMG-HSQC experiments were performed as described before (*26*). To reduce resonance offset effects, the ^1H carrier was placed at the center of the amide proton resonances in both experiments. Spectra were recorded as 52 × 512 complex points (RXR) and 128 × 512 complex points (RAR) with spectral widths of 2000 and 8000 Hz in t_1 (^{15}N) and t_2 (^1H), respectively. Experiment times per spectrum were 1 and 4 h, acquiring 16 and 32 scans per FID for RXR and RAR, respectively. The contribution of conformational exchange to the $^1H^N$ transverse relaxation rates (R_{ex}) was identified from the ratio of the peak intensities I_{CPMG} and I_{ref} in the CPMG-enhanced and "regular" HSQC spectra. Signal intensity loss in the "regular" HSQC due to transversal relaxation in the INEPT periods can be described by $I_{ref} = I_0\, e^{-tR_{tot}}$, with $R_{tot} = R_{DD+CSA} + R_{ex}$. I_o stands for the starting intensity, t for the time during which relaxation is active and R_{tot} for the total relaxation rate which can be described as the sum of relaxation induced by dipole−dipole and chemical shift anisotropy interactions (R_{DD+CSA}) and relaxation induced by chemical exchange (R_{ex}). Due to the application of CPMG-derived pulse trains during the INEPT transfer periods in the CPMG-HSQC, R_{ex} is significantly reduced (*26*, *27*). Therefore the signal intensity loss can be approximated by $I_{CPMG} = I_o\, e^{-tR_{DD+CSA}}$. Rearrangement shows that $I_{CPMG}/I_{ref} = \exp(R_{ex}t)$.

RESULTS

NMR can be used to probe dynamics on time scales ranging from seconds to picoseconds. The measurement of ^{15}N spin relaxation rates for proteins is a well-established tool to obtain information about (sub)nanosecond time scale motion. Furthermore, millisecond to microsecond motions can be identified from an increase in the transverse relaxation rate due to conformational exchange (*28*, *29*). This additional relaxation contribution originates from time-dependent perturbations of the environment of a particular nucleus, modulating its chemical shift. When the rate of the exchange process, k_{ex}, exceeds the difference in chemical shift, $\delta\omega$, ($k_{ex} > \delta\omega$; fast exchange limit), a single resonance line is observed, with a line width increased by the conformational exchange process.

Transverse relaxation contributions due to conformational exchange were determined experimentally from the decay rates of ^{15}N CPMG T_2 experiments and from a ^1H constant time differential transverse relaxation filter (see Materials and Methods). Since the motions experienced by an amide proton and its directly attached nitrogen atom are intimately related, ^1H and ^{15}N exchange-mediated relaxation rates report on the same motional processes. Therefore, combined analysis allows for a more exhaustive identification of intermediate time scale dynamics as the chemical shift perturbation of one of the two nuclei, and hence its relaxation contribution may be small. Furthermore, it reduces the possibility that increases in transversal relaxation rates caused by anisotropic reorientation will be mistakenly identified as exchange broadening.

Millisecond to Microsecond Motions in RXR. Figure 2A shows the ^{15}N transverse relaxation rates (R_2) of the backbone nitrogen nuclei, as a function of residue number. Empty slots indicate residues that have not been assigned (133, 134, 143, 153, 184−188), or were excluded due to slow exchange (171).

The overall tumbling of the molecule in solution determines the R_2 values of the residues that are part of the helices (the most rigid part of the protein). In the case of isotropic tumbling, any deviating rates, either lower or higher, arise from additional internal dynamics. Dynamics on the nano- to picosecond time scale reduce the observed relaxation rate, as is observed for residue 144 and the C-terminal residues 207−209. Millisecond to microsecond time scale movements cause R_2 values to be higher. The largest R_{ex} contributions to R_2 are seen for a stretch of residues 174, 175, 177−180, 181, and 183, grouped around the second metal-coordinating cysteine of the second finger. Residues 149, part of the first zinc finger, and 169, part of the linker connecting the two zinc finger modules of the DBDs, show elevated R_2 values as well.

The peak intensity ratios of the CPMG-HSQC and HSQC spectra are plotted as a function of residue number. Residues not affected by conformational exchange have the same intensities in the two spectra, yielding a ratio of one. Signals with significantly higher values than 1.0 are affected by conformational exchange, as can be seen most clearly for residues 175, 177−179, and to a lesser extent 172 and 181. The level of significance is defined as a 2σ window around the mean, calculated from all residues except 175 and 177, which were rejected by Dixons Q-test for outliers.

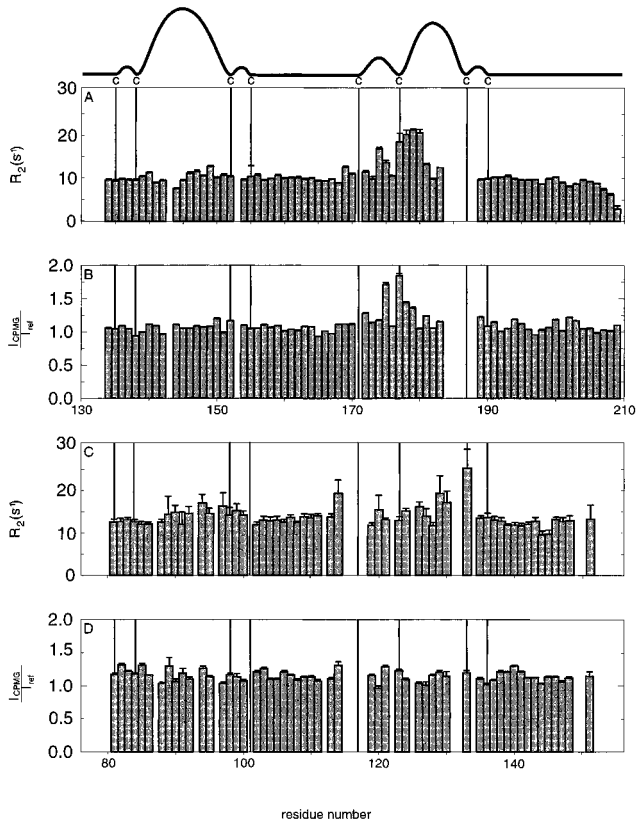

FIGURE 2: Bar graphs of the transverse relaxation data of RXR and RAR DBDs as a function of residue number. In (A) and (C) the ^{15}N R_2 values are plotted for RXR and RAR, respectively. In (B) and (D), I_{CPMG}/I_{ref} is plotted for RXR and RAR, respectively. At the top of the graph a schematic overview is given of the structure of the DBDs. In each of the panels, vertical lines indicate the positions of the cysteine residues.

Millisecond to Microsecond Motions in RAR. In RAR DBD conformational exchange is observed as well, although the effects are less pronounced. Dynamics on the milli- to microsecond time scale was found in both zinc fingers as can be seen from the ^{15}N transverse relaxation rates (Figure 2C). Residues 94, 97, and 99 of the first zinc finger and residues 120, 124, 126, 129, 130, and 133 of the second zinc finger were identified. Furthermore, residue 114, which is part of the linker between the second helix and the D-box of RAR, has a significant R_{ex} contribution. The only residues exhibiting nano- to picosecond time scale internal dynamics are 144 and 145, the terminal residues of the second helix. The results of the "regular" and CPMG-HSQC experiments are presented in Figure 2D. No residues exhibit values of I_{CPMG}/I_{ref} which fall outside the 2σ window.

A number of residues were excluded because they were severely overlapping (112, 122), because they were too weak to be reliably assigned, or because they could not be assigned at all (75−80, 87, 93, 96, 101, 115−118, 125, 131, 134, 149, 150, 152−163).

DISCUSSION

The two zinc fingers of RAR and, in particular, the second zinc finger of RXR, are highly mobile. For RXR the residues most strongly affected are 174, 175, and 177−180, centered around the second zinc-coordinating cysteine. Smaller effects are observed for 171 (slow exchange), 169, 172, 181, and 183, also belonging to the second zinc finger region. For the second zinc finger of RAR, some motion is observed around the second zinc-coordinating cysteine (a small effect on residues 120, 124, and 126) and more pronounced flexibility around the third coordinating cysteine (residues 129, 130, and 133). For RAR the motion of the first zinc finger (94, 97, and 98) is more pronounced than for the corresponding region in RXR, where only minor effects are observed for residues 144 (fast motion) and 149. In general, the R_2 values of RAR are larger than for RXR. A possible explanation could be a general enhancement of transverse relaxation rates due to chemical exchange, as was reported by Palmer et al. (*30*) for a fibronectin type III domain. If aggregation of the proteins causes the different transverse relaxation behavior, the tendency to aggregate is larger for RAR than for RXR since the R_2 values are higher at lower concentrations. In both proteins there is a stretch of residues in the second zinc finger (184−188 in RXR and 115−118 in RAR) of which the signals are not visible in the NMR spectra. Since in the experiments care has been taken to minimize saturation of the water signal, these signals are most likely broadened beyond detection due to conformational exchange and not due to saturation transfer from the solvent.

There is a long-standing debate about whether the disorder found in the solution structures of nuclear receptors is caused by flexibility (*5*−*8*, *17*, *18*). For GR (*22*) and RXR (*19*), NMR measurements indicated hardly any nano- to picosecond motions. The data presented here provide the first experimental evidence that, at least for RXR and RAR, the poorer definition of the structures in these regions is due to extensive milli- to microsecond dynamics.

There is a striking correlation between the main mobile regions in RAR and RXR and the reported dimer interfaces of these proteins, when complexed with a partner receptor molecule and DNA. In RXR the larger part of the D-box and the tip of the second zinc finger are highly mobile. The D-box forms the dimer interface of RXR when in complex with RAR or TR on DR5 or DR4, respectively. The dimerization region in RAR and TR is the tip of the first finger (*15*, *21*). Figure 3 shows a model of the RXR−RAR (DR5) complex, constructed by docking the proteins in the center of their respective half-sites. The model shows how the flexible regions of RXR and RAR point toward each other to constitute the dimer interface.

In the dimeric complexes on DR1 and DR2, the tip of the second zinc finger of the upstream RXR interacts with CTEs of RXR and RAR, respectively (*15*). Furthermore, RAR forms a heterodimer with RXR on DR1 (*13*). In contrast to most class II heterodimeric complexes, RXR is the downstream component in this complex. If the protein assembly in this complex resembles that of the homodimeric RXR on DR1, the tip of the second finger makes up the protein−protein interface in RAR. In RXR the three terminal residues exhibit high-frequency motion, which is often observed for proteins. Whether the CTE of RAR is flexible is not clear since residues 152−163 are not visible in the spectra, which can be either due to fast exchange with the solvent or due to exchange broadening.

For GR (*9*) and ER (*10*), it was observed that differences in ordering of the second zinc finger region between the solution and crystal structures arise upon complex formation.

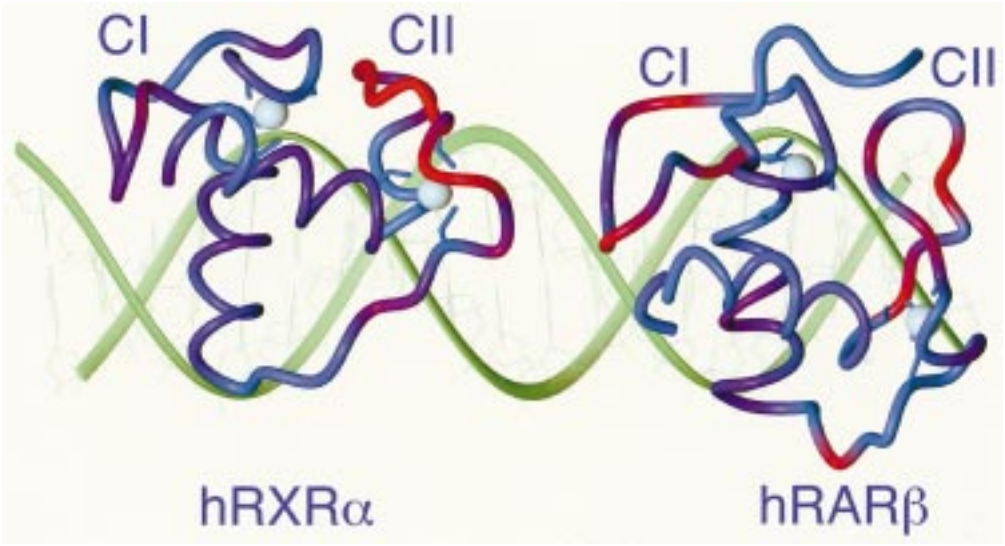

FIGURE 3: Ribbon diagram of the 3D structures of RXR (left; taken from ref *21*) and RAR (right; taken from ref *20*) in an approximate orientation reported for the RXR/RAR heterodimeric complex on DR5 (represented by B-form DNA (*17*, *21*)). Balls indicate the zinc ions. CI and CII indicate the first and second zinc fingers, respectively. The ribbon is color-coded according to the extent of flexibility. The color spectrum ranges from blue (rigid) to red (extensive mobility). This picture is created with the program molmol (*33*).

A partial folding transition is supported by thermodynamic analyses of the GR complex (*31*), in which it is concluded that approximately 18 residues of GR become ordered when binding DNA. Recently, it has been proposed that allosteric conformational changes, induced by DNA, allow the formation of the dimer interface and protein−protein interactions with co-activators (*7*).

RXR ordering of the entire second zinc finger region, similar to GR and ER, upon assembly of the RXR-TR (DR4) complex has been observed (*19*, *21*). Furthermore, it was found that complexes of RAR and RXR on differentially spaced response elements produce distinct transcriptional responses (*13*, *32*), whereby release of the co-repressor N-coR upon treatment with hormone is allosterically regulated by the DNA response elements (*13*). The reported flexibility would facilitate conformational changes associated with this regulation.

In conclusion, we have demonstrated that the major dimerization areas in RAR and RXR display the largest exchange-mediated relaxation rates due to millisecond to microsecond time scale dynamics. This flexibility in the dimerization domains may facilitate transitions to a protein conformation that allows for more optimal protein−protein interactions, and is consistent with an induced fit mechanism upon ternary complex formation. Such a mechanism would also explain the more extensive flexibility observed for RXR when compared with RAR, since RXR must be able to comply with various partners in different orientations.

ACKNOWLEDGMENT

We would like to thank Dr. P. E. Wright for a copy of their manuscript prior to publication.

REFERENCES

1. Mangelsdorf, D. J., Thummel, C., Beato, M., Herrlich, P., Schütz, G., Umesono, K., Blumberg, B., Kastner, P., Mark, M., Chambon, P., and Evans, R. M. (1995) *Cell 83*, 835−839.
2. Mangelsdorf, D. J., and Evans, R. M. (1995) *Cell 83*, 841−850.
3. Beato, M., Herrlich, P., and Schütz, G. (1995) *Cell 83*, 851−857.
4. Zilliacus, J., Wright, A. P. H., Carlstedt-Duke, J., and Gustafsson, J. Å. (1995) *Mol. Endocrinol. 9*, 389−400.
5. Baumann, H., Paulsen, K., Kovács, H., Berglund, H., Wright, A. P. H., Gustafsson, J. Å., and Härd, T. (1993) *Biochemistry 32*, 13463−13471.
6. Van Tilborg, M. A. A., Bonvin, A. M. J. J., Hård, K., Davis, A. L., Maler, B., Boelens, R., Yamamoto, K. R., and Kaptein R. (1995) *J. Mol. Biol. 247*, 689−700.
7. Van Tilborg, M. A. A. (1998) Ph.D. Thesis, *Utrecht University*, Utrecht, The Netherlands.
8. Luisi, B. F., Xu, W. X., Otwinowski, Z., Freedman, L. P., Yamamoto, K. R., and Sigler, P. B. (1991) *Nature 352*, 497−505.
9. Schwabe, J. W. R., Chapman, L., Finch, J. T., Rhodes, D., and Neuhaus, D. (1993) *Structure 1*, 187−204.
10. Schwabe, J. W. R., Chapman, L., Finch, J. T., and Rhodes, D. (1993) *Cell 75*, 567−578.
11. Schwabe, J. W. R., Chapman, L., and Rhodes, D. (1995) *Structure 3*, 201−213.
12. Mangelsdorf, D. J., Umesono, K., and Evans, R. M. (1994) in *The Retinoids*: *Biology*, *Chemistry*, *and Medicine* (Sporn, M. B., Roberts, A. B., and Goodmann, D. S., Ed.) pp 319−349, Raven Press Ltd., New York.
13. Kurokawa, R., DiRenzo, J., Boehm, M., Sugarman, J., Gloss, B., Rosenfeld, M. G., Heyman, R. A., and Glass, C. K. (1994) *Nature 371*, 528−531.
14. Kliewer, S. A., Umesono, K., Noonan, D. J., Heyman, R. A., and Evans, R. M. (1992) *Nature 358*, 771−774.
15. Zechel, C., Shen, X. Q., Chen, J. Y., Chen, Z. P., Chambon, P., and Gronemeyer, H. (1994) *EMBO J. 13*, 1425−1433.
16. Perlmann, T., Rangarajan, P. N., Umesono, K., and Evans, R. M. (1993) *Genes Dev. 7*, 1411−1422.
17. Zechel, C., Shen, X. Q., Chambon, P., and Gronemeyer, H. (1994) *EMBO J. 13*, 1414−1424.
18. Lee, M. S., Kliewer, S. A., Provencal, J., Wright, P. E., and Evans, R. M. (1993) *Science 260*, 1117−1121.
19. Holmbeck, S. M. A., Foster, M. P., Casimiro, D. R., Sem, D. S., Dyson, H. J., and Wright, P. E. (1998) *J. Mol. Biol. 281*, 271−284.
20. Knegtel, R. M. A., Katahira, M., Schilthuis, H., Boelens, R., Eib, D., Van der Saag, P. T., and Kaptein, R. (1993) *J. Biomol. NMR 3*, 1−17.
21. Rastinejad, F., Perlmann, T., Evans, R. M., and Sigler, P. B. (1995) *Nature 375*, 203−211.

22. Berglund, H., Kovács, H., Dahlman-Wright, K., Gustafsson, J. Å., and Härd, T. (1992) *Biochemistry 31*, 12000−12011.
23. Delaglio, F., Grzesiek, S., Vuister, G. W., Zhu, G., Pfeifer, J., and Bax, A. (1995) *J. Biomol. NMR 6*, 277−293.
24. Wüthrich, K., (1986) *NMR of proteins and nucleic acids*, Wiley, New York, NY.
25. Vis, H., Vorgias, C. E., Wilson, K. S., Kaptein, R., and Boelens, R. (1998) *J. Biomol. NMR 11*, 265−277.
26. Mulder, F. A. A., Spronk, C. A. E. M., Slijper, M., Kaptein, R., and Boelens, R. (1996) *J. Biomol. NMR 8*, 223−228.
27. Carr, H. Y., and Purcell, E. M. (1954) *Phys. Rev. 94*, 630−638.
28. Palmer, A. G., III, Williams, J., and McDermott, A. (1996) *J. Phys. Chem. 100*, 13293−13310.
29. Mulder, F. A. A., Van Tilborg, P. J. A., Kaptein, R., and Boelens, R. (1998) *J. Biomol. NMR* (in press).
30. Akke, M., Liu, J., Cavanagh, J., Erickson, H. P., and Palmer, A. G., III (1998) *Nat. Struct. Biol. 5*, 55−59.
31. Spolar, R. S., and Record, M. T. (1994) *Science 263*, 777−784.
32. Kurokawa, R., Söderström, M., Hörlein, A., Halachmi, S., Brown, M., Rosenfeld, M. G., and Glass, C. K. (1995) *Nature 377*, 451−454.
33. Koradi, R., Billeter, M., and Wüthrich, K. (1996) *J. Mol. Graph. 14*, 51−55.

BI982526Q